Dynamical and Chemical Features of a Cutoff Low over Northeast China in July 2007: Results from Satellite Measurements and Reanalysis

LIU Chuanxi[1] (刘传熙), LIU Yi[*1] (刘 毅), Xiong LIU[2], and Kelly CHANCE[2]

[1]*Key Laboratory of Middle Atmosphere and Global Environment Observation, Institute of Atmospheric Physics,*

Chinese Academy of Sciences, Beijing 100029

[2]*Harvard-Smithsonian Center for Astrophysics, Cambridge, Massachusetts, USA*

ABSTRACT

The European Centre for Medium-Range Weather Forecasts Re-Analysis Interim (ERA-Interim) meteorology and measurements from the Microwave Limb Sounder, High Resolution Dynamics Limb Sounder, and Ozone Monitoring Instrument onboard the Earth Observing System Aura satellite were applied to analyze the dynamical and chemical features of a cutoff low (COL) event over northeast China in early July 2007. The results showed the polar stratospheric origin of an upper-level warm-core cyclone at 100–300 hPa, associated with a funnel-shaped tropopause intruding into the mid-troposphere just above the COL center. The impacts of the stratospheric intrusion on both column ozone and ozone profiles were investigated using satellite measurements. When the intensity of the COL peaked on 10 July 2007, the total column ozone (TCO) increase reached a maximum (40–70 DU). This could be dynamically attributed to both the descent of the tropopause ($\sim$75%) and the downward transport of stratospheric ozone across the tropopause ($\sim$25%). Analysis of the tropospheric ozone profiles provided evidence for irreversible transport/mixing of ozone-rich stratospheric air across the tropopause near the upper-level front region ahead of the COL center. This ozone intrusion underwent downstream transport by the upper tropospheric winds, leading to further increase in TCO by 12–16 DU over broad regions extending from east China toward the northern Japan Sea via South Korea. Meteorological analysis also showed the precedence of the stratospheric intrusion ahead of the development of cyclones in the middle and lower troposphere.

Key words: stratosphere-troposphere exchange, cutoff low, tropopause, ozone, satellite observation

1. Introduction

A cutoff low (COL) is a closed upper-tropospheric low-pressure system that is completely detached (cut off) from its polar source and extends to the south of the mid-latitude westerly mean flow as a result of the deepening of a high-level trough (Palmén and Newton, 1969; Gimeno et al., 2007). Along with its slowly southward excursion, a COL usually maintains its polar characteristics [e.g., low temperature and high potential vorticity (PV)] in the middle and upper troposphere. In an intense COL event, there could be a "tropopause funnel" dipping as low as the mid-troposphere (Palmén, 1949; Peltonen, 1963). A funnel-shaped tropopause is also usually associated with substantial descent of stratospheric air, producing a warm core in the lower stratosphere just above the pronounced "cold dome" in the troposphere (e.g., Sato, 1951). As a result, an intense COL event typically causes pronounced stratospheric intrusion into the upper troposphere (e.g., Holton et al., 1995; Stohl et al., 2003; Sprenger et al., 2007), which could be responsible for an unusual increase in the tropospheric ozone concentrations below (Ancellet et al., 1994; Kentar-

---

*Corresponding author: Yi LIU, liuyi@mail.iap.ac.cn

chos et al., 2000). Previous studies have suggested that both convective mixing and the radiative erosion of the funnel-shaped tropopause should be the principal mechanisms responsible for stratosphere-troposphere exchange (STE) in a COL event (Price and Vaughan, 1993; Wirth, 1995). It has also been proposed that a decaying COL could be a preferable condition for massive stratospheric intrusions throughout the COL lifecycle (Gouget et al., 2000).

Considering the marked change in PV across the tropopause, stratospheric intrusion related to a COL leads to an isolated area of high isentropic PV originating from the polar stratospheric reservoir. Therefore, PV theory can be used to identify and explain the formation and evolution of a COL. Hoskins et al. (1985) proposed a conceptual duality between cutoff cyclones and blocking anticyclones from the viewpoint of PV anomalies near the tropopause (positive isentropic PV anomalies correspond to cutoff cyclones, whereas negative anomalies correspond to blocking anticyclones). According to the well-established "PV thinking" perspective (Hoskins et al., 1985), a pronounced positive PV anomaly at the upper level might be phase-locked to rapid cyclogenesis below. Extensive observations have also indicated that a cold vortex in a COL event sometimes develops above a low-level anticyclone, leading to a weakening of the surface anticyclone or even strengthening of a surface cyclone (e.g., Hsieh, 1949; Palmén, 1949; Nieto et al., 2005, 2008). Therefore, study of the stratospheric intrusion related to a COL and its tropospheric consequences might provide a clue to understanding the mechanism responsible for dynamical couplings between the stratosphere and troposphere.

In recent decades, a number of studies have examined the climatology of COLs in the Northern Hemisphere (NH) based on an object analysis of 500-hPa pressure surfaces (Bell and Bosart, 1989; Parker et al., 1989) and 200-hPa (Kentarchos and Davies, 1998). Most COLs last for 2–3 days, and very few last for >10 days. It has also been shown that COL events occur more often in summer than in winter and generally form in preferred geographical regions. According to their locations of occurrence, Price and Vaughan (1992) divided COL events into three categories: polar vortex, polar, and subtropical. Recently, Nieto et al. (2005, 2008) provided a multi-decadal climatology of COLs in the NH and confirmed previous conclusions on their duration and seasonal cycle. They also concluded that the three preferred areas of COL occurrence in the NH are southern Europe and the eastern Atlantic coast, the eastern north Pacific, and the northern China–Siberian region extending to the northwest Pacific coast, with the European region be-

ing the most active.

Due to its preferred occurrence in Northeast China and cold-core feature throughout the middle and upper troposphere, a COL is traditionally called a "northeast cold vortex" in Chinese meteorological literature. As a result of their long-term persistence, cold vortices often cause cold spells and heavy rainfall, which account for 20%–60% of the total precipitation in the warm season (May–September; Zhang et al., 2008) and ∼25% of annual mean precipitation in North China (Hu et al., 2010). Consequently, an intense COL event might lead to severe flooding, especially in late spring and early summer (from May to June; Tao, 1980; Zhao et al., 2007). However, due to the lack of local stratospheric soundings in this region, little academic attention has been given to the stratospheric intrusion features of COLs. These have been substantially investigated for similar events over Europe and North America. Yang and Lü (2003) quantified the mass STE associated with an intense COL event over Eastern China using a mesoscale model. Recent advances in remote sensing provide us unprecedented opportunities for bird's-eye views of COLs over a broad area and for detection of fine structures throughout their life cycles.

In this study, we investigated the stratospheric intrusion of an intense COL event in early July 2007 and its impact on (1) the thermal structure and ozone concentration in the upper troposphere and lower stratosphere (UTLS) and (2) the dynamical evolution of low-level cyclones. This article is organized as follows: section 2 introduces meteorological data and satellite observations. Section 3 describes the meteorological evolution of the COL event in question. Features of stratospheric intrusion and its impact on both column ozone and ozone profiles are presented in section 4. Section 5 discusses the potential relationship between the stratospheric intrusion and the strengthening of low-level cyclones. The main conclusions are summarized in section 6.

2. Meteorological reanalysis and satellite observations

We used the European Center for Medium-range Weather Forecasts (ECMWF) Interim reanalysis (ERA-Interim) (Simmons et al., 2007a, b), a new global reanalysis dataset (ranging from 1989 to now, four times per day), for meteorological analysis. The ERA-Interim data had a horizontal resolution of 1.5°×1.5° and 37 vertical pressure levels extending from 1000 to 1 hPa. The PV isoline from ERA-Interim data was used to analyze the variations in the dynamical tropopause [2 PV Units (PVU), 1

PVU $= 1.0 \times 10^{-6}$ K m^2 kg^{-1} s^{-1}], and the isentropic PV contours at 330 K were also used to identify the downward intrusion of stratospheric air masses (see section 5). The temperature from ERA-Interim reanalysis is used to calculate the thermal tropopause height based on World Meteorological Organization (WMO) definition (WMO, 1957). Comparison shows that the ERA-Interim tropopause agrees well with the result from National Center for Environmental Prediction (NCEP) final (FNL) operational global analysis data (not shown). In this study, location of lapse-rate tropopause is also contrasted with that of PV-based dynamic tropopause (Figs. 3, 5, and 9).

The Microwave Limb Sounder (MLS; Waters et al., 2006) on the Earth Observing System Aura spacecraft, which was launched on 15 July 2004, observed thermal microwave limb emission in five spectral regions from 118 GHz to 2.5 THz. In MLS level-2 products, there are six levels in the UTLS region between 200 and 50 hPa: 177, 146, 121, 100, 82, and 68 hPa. Details regarding the use of MLS level-2 products were provided in an MLS data quality and description document (Livesey et al., 2007, 2011). Livesey et al. (2008) evaluated the accuracy of O_3 and CO concentrations between 215 and 100 hPa produced by the MLS version 2.2 retrievals. The O_3 accuracy was estimated at ∼40 ppbv +5% (∼20 ppbv +20% at 215 hPa), and the CO accuracy was estimated at ∼30 ppbv +30% for pressures of 147 hPa and less. Generally, according to previous validation study (Livesey et al., 2008), O_3 and CO products from MLS measurements are scientifically useful in the UTLS at pressures of 215 hPa and smaller. Therefore, in the present study, temperature and mixing ratios of O_3 and CO from the MLS Level-2 product (version 3) above 215 hPa were used to illustrate the stratospheric ozone intrusion associated with the tropopause funnel.

The High Resolution Dynamics Limb Sounder (HIRDLS; Gille et al., 2003) is also onboard the EOS-Aura spacecraft. It measures atmospheric limb emissions from 6.12 to 17.76 mm in 21 spectral channels to obtain vertical profiles of temperature, pressure, mixing ratios of atmospheric constituents (e.g., O_3, HNO_3, and aerosol extinction), and cloud-top pressures. The HIRDLS was designed to sound the upper troposphere, stratosphere, and lower mesosphere with high vertical and horizontal resolution, obtaining global coverage (including the poles) during both day and night (Gille et al., 2003, 2008). The horizontal along-track (latitudinal) sampling is approximately 1° (75–100 km) and the vertical resolution is as high as 1 km. Nardi et al. (2008) compared HIRDLS ozone retrievals (V2.04.09) with ozonesondes, ground-based lidar, and airborne lidar measurements. Their com-

parison indicated that the ozone retrieval of this version was recoverable between1 and 100 hPa at middle and high latitudes, where the accuracy was estimated to be generally 5%–10% in the middle and upper stratosphere (1–50 hPa) and 10%–20% in the lower stratosphere (50–100 hPa). Comparisons confirmed that that HIRDLS was capable of resolving fine vertical ozone features (1–2 km) in the region between 1 and 50 hPa. Gille et al. (2008) compared the HIRDLS temperatures (V2.04.09) with measurements from radiosondes, lidars, and other satellite and outputs from ECMWF analysis. They showed that the HIRDLS temperatures are 1–2 K warm, which is within ±2 K of standards, from the upper troposphere (200 hPa) to the upper stratosphere (10 hPa) in extratropics. These comparisons were recently updated for version 5 products by the HIRDLS Team (2010). The HIRDLS temperature is within 0.5 K of the high-resolution radiosondes from ∼300 hPa to above 10 hPa, with larger differences below 300 hPa. The HIRDLS ozone precision is 100–300 ppbv (∼1%–4%) between 1–100 hPa, 50–100 ppbv (∼25% at mid-latitudes and 5%–15% at high latitudes) between 100–260 hPa, and 100–300 ppbv (∼4%–10%) between 0.5–1 hPa. In this study, the V5 HIRDLS temperature and ozone were used together with the MLS products.

The Ozone Monitoring Instrument (OMI), also onboard the Aura satellite, measures direct sunlight and backscattered light from the Earth's atmosphere in the wavelength range 270–500 nm (Levelt et al., 2006). It provides daily global coverage, except for the polar night region, with a nadir spatial resolution of 13 km ×24 km (lat × lon). We used the retrieved total column ozone (TCO) and the ozone profile from the OMI (Liu et al., 2010a) to quantify the influence of the COL on the total column ozone and irreversible STE of ozone. Profiles of partial ozone columns were retrieved from the surface to ∼60 km in 24 layers from OMI radiances using the optimal estimation technique (Liu et al., 2010a). In addition to the TCO, the stratospheric and tropospheric column ozone were integrated from the retrievals with the use of daily NCEP tropopause data. Retrieval errors (including both precision and smoothing errors) varied from 1–6% in the middle stratosphere to 6%–35% in the troposphere. In total, stratospheric, and tropospheric column ozone could be retrieved with errors typically in the few DU range at solar zenith angles <80°. The OMI ozone profiles agreed closely with MLS data; global mean biases were within 2.5% between 0.2–100 hPa and within 5%–10% between 100–200 hPa. The standard deviations of the differences were 3.5%–5% between 1–50 hPa and 8%–15% between 50–200 hPa (Liu et al., 2010b). Stratospheric column ozone (SCO)
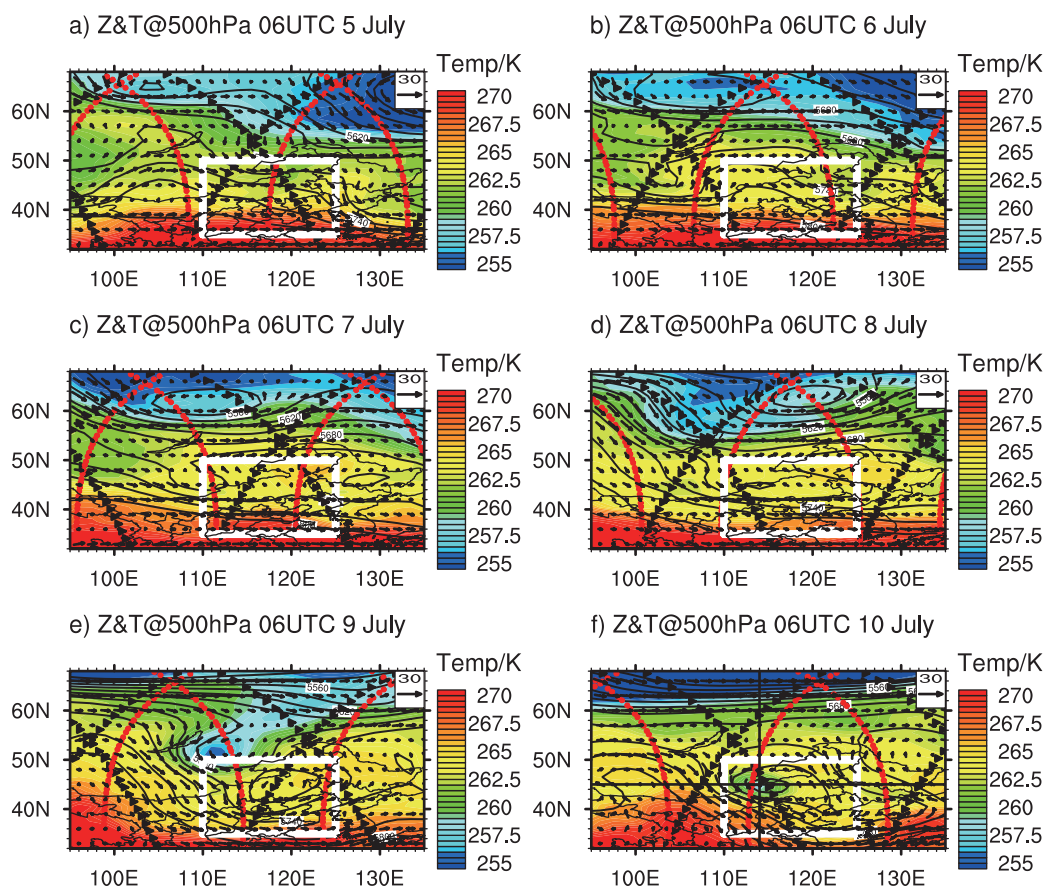
Fig. 1. ERA-Interim temperature (shaded: K) and geopotential height (contour: m) together with wind vectors (m s^{-1}) at 500 hPa pressure surface: (a) 0600 UTC 5 July; (b) 0600 UTC 6 July; (c) 0600 UTC 7 July; (d) 0600 UTC 8 July; (e) 0600 UTC 9 July; (f) 0600 UTC 10 July 2007. Locations of Microwave Limb Sounder (MLS) and High Resolution Dynamics Limb Sounder (HIRDLS) profiles are marked by black triangles and red dots. Place of the cutoff low (COL) occurrence is indicated by a white box. The geopotential height contour ranges from 5500 to 5800 m, with the interval of 30 m.

also agreed closely with MLS data ($-0.6\%\pm2.8\%$). For the northern mid-latitude summer, OMI ozone profiles in the UTLS and troposphere agreed with ozonesonde observations to within 5%, with standard deviations of the differences of 10%–18%; tropospheric column ozone agreed closely with ozonesondes (-1.6 ± 5.4 DU). Validation with aircraft measurements in the UTLS (100–300 hPa) showed that OMI retrievals generally agree with aircraft data to within $\pm50\%$ for ozone quantities >200 ppbv. Therefore, they can capture the synoptic-scale ozone gradients associated with strong potential vorticity gradients (Pittman et al., 2009).

3. Meteorological evolution of the July 2007 COL event over northern China

As discussed in section 1, previous studies have shown that a COL is an upper-level cyclone with a cold core throughout the troposphere, but a warm core in the lower stratosphere. In this section, the ERA-Interim dataset was applied to analyze the dynamical and thermal structures of the COL event over northern China in early July 2007.

Figure 1 shows the daily evolution (0600 UTC each day) of temperature and geopotential height at 500-hPa pressure surface before and during the COL occurrence (5–10 July 2007), together with the locations of MLS (triangles) and HIRDLS (dots) profiles on each day. On 5 July 2007, a shallow ridge occurred over northern Mongolia as a result of warm advection to the south of the Baikal region (Fig. 1a). Due to the persistent development and eastward propagation of the Mongolian ridge, a growing trough extended from Siberia to northern China during 6–7 July 2007 (Figs. 1b and c). The southeastward extension of the cold trough led to pronounced cooling in Mongolia
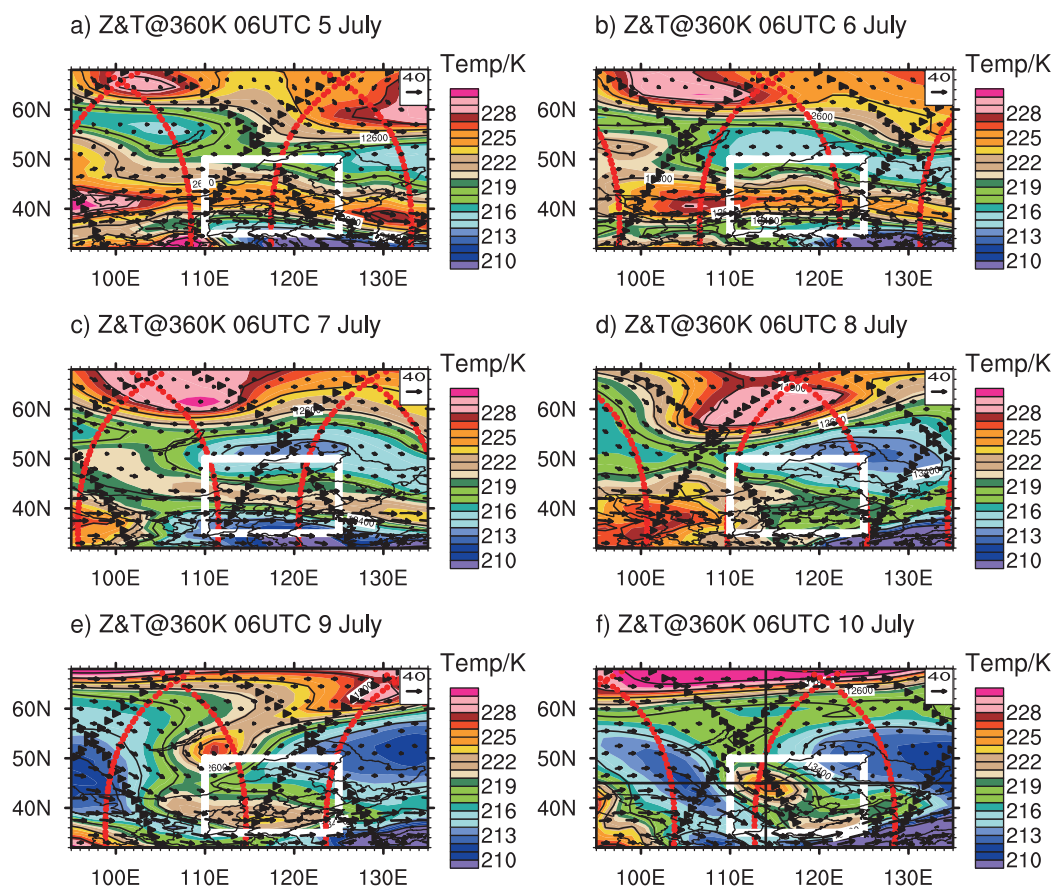
Fig. 2. Same as Fig. 1, but for the 360 K isentropic surface. The geopotential height contour ranges from 11000 to 15000 m, with the interval of 400 m.

and northern China, producing a closed cyclone in the middle troposphere over northeast China on 8 July 2007 (Fig. 1d, box). With the eastward movement of another intense ridge from behind, a large pocket of cold air mass was stripped from the polar cold pool on 9 July 2007 (Fig. 1e) and merged with the existing closed cyclone (Fig. 1d), leading to an intense COL over northern China (Fig. 1f).

Figure 2 is the same as Fig. 1, except for the 360-K isentropic surface, which represents the lowermost stratosphere. The horizontal distribution of 360-K temperature was significantly different from that in the middle troposphere (compare Fig. 2 with Fig. 1). As shown in Figs. 2a–d, in a calm state (5–8 July 2007), the temperature north of 60°N was much higher than that between 45°N and 60°N. Moreover, the 360-K temperature between 45°N and 60°N was quite sensitive to the vertical undulation of the atmosphere. For example, at 0600 UTC 5 July 2007, the temperature along 55°N latitude in the region with a weak ridge (over the Lake Baikal) was ∼5 K cooler than that in the region with a shallow trough (Fig. 2a). On 9 July

2007, with the eastward movement of an intense ridge (as in the situation at 500 hPa shown in Fig. 1e), a pronounced warm trough was stripped off the polar warm pool and extended southward toward Mongolia (Fig. 2e). On 10 July 2007, the elongated warm trough was completely detached from its polar origin and reached northern China, producing a closed warm-core cyclone above the low-level cold cyclone (compare Figs. 1f with 2f).

4.   Features of stratospheric intrusion

In this section, based on the ERA-Interim meteorological data and satellite observations, we focus on the thermal and dynamical structures of the funnel-shaped tropopause (also known as the "tropopause funnel") in the COL event and their impact on local TCO and ozone profiles.

4.1   *Origin of the stratospheric intrusion*

Figure 3 shows the cross-sections of temperature, potential temperature, zonal wind speed, PV isolines
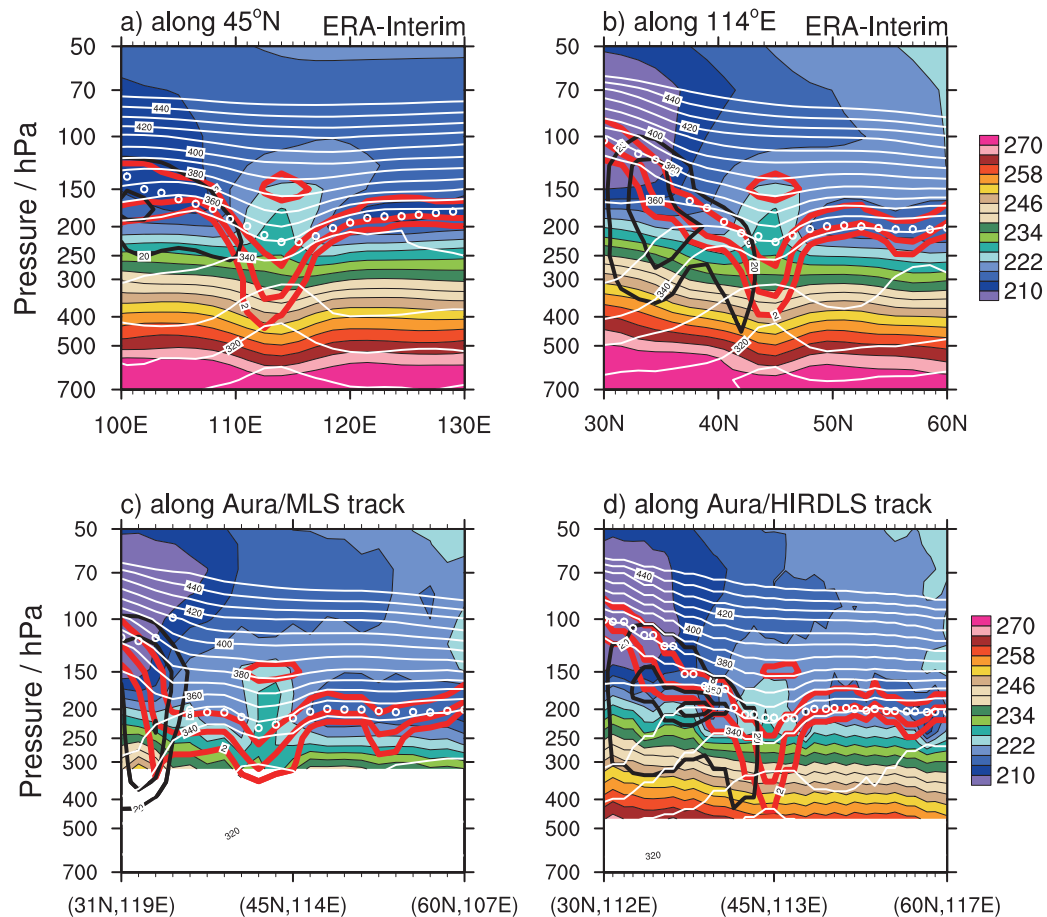
Fig. 3. (top) Zonal and meridional cross sections of ERA-Interim temperature (shaded: K) and potential temperature (white contour: K) along (a) 45°N and (b) 114°E at 0600 UTC 10 July 2007. (bottom) Cross-sections of MLS/HIRDLS temperature (shaded: K) and ERA-Interim potential temperature (white contour: K) along satellite tracks: (c) MLS; (d) HIRDLS. The zonal wind speed >20 m s^{-1} is shown by black solid contours with intervals of 10 m s^{-1}. ERA-Interim potential vorticity (PV) isolines [2, 4, and 8 PV units (PVU)] are overlaid representing the location of dynamical tropopause (red bold solid line). Thermal tropopause from ERA-Interim reanalysis is also marked with the white circles.

of 2, 4, and 8 PVU, and thermal tropopause along transects crossing the center of the COL at 0600 UTC 10 July 2007 based on ERA-Interim data and satellite profiles from MLS and HIRDLS instruments. Both the PV isolines and thermal tropopause show similar features. In particular, the dynamical tropopause (represented by the 2-PVU PV isoline) above the area of COL occurrence dipped below the thermal tropopause, reaching as low as 400 hPa and producing a pronounced "tropopause funnel" (Figs. 3a, b, and d). Meanwhile, the convergence of the potential temperature contours near the "tropopause funnel" region suggests the stabilization of the UTLS region near the COL. In addition, both ERA-Interim meteorological data and satellite observations show that the isotherms

above the tropopause funnel bulged up, indicating that the COL in the UTLS region ranging from 250 to 100 hPa was 3–4 K warmer than its surroundings (see also Fig. 2f). Previous studies have suggested that the warm-core of upper-level cyclone is probably related to the warming associated with the formation of the tropopause funnel (e.g., Sato, 1951). Figures 3b–d show the 218 K isothermal is traceable as far as the polar stratosphere (e.g., 70–150 hPa around 60°N), indicating a polar stratospheric origin of the downward transport and the resulting upper-level warm core.

Figure 4 displays the 6-h evolution (between 0000 UTC 9 July and 0600 UTC 10 July) of the stratospheric intrusion. For example, during the first 12 h (0000–1200 UTC 9 July), as a result of the rapid
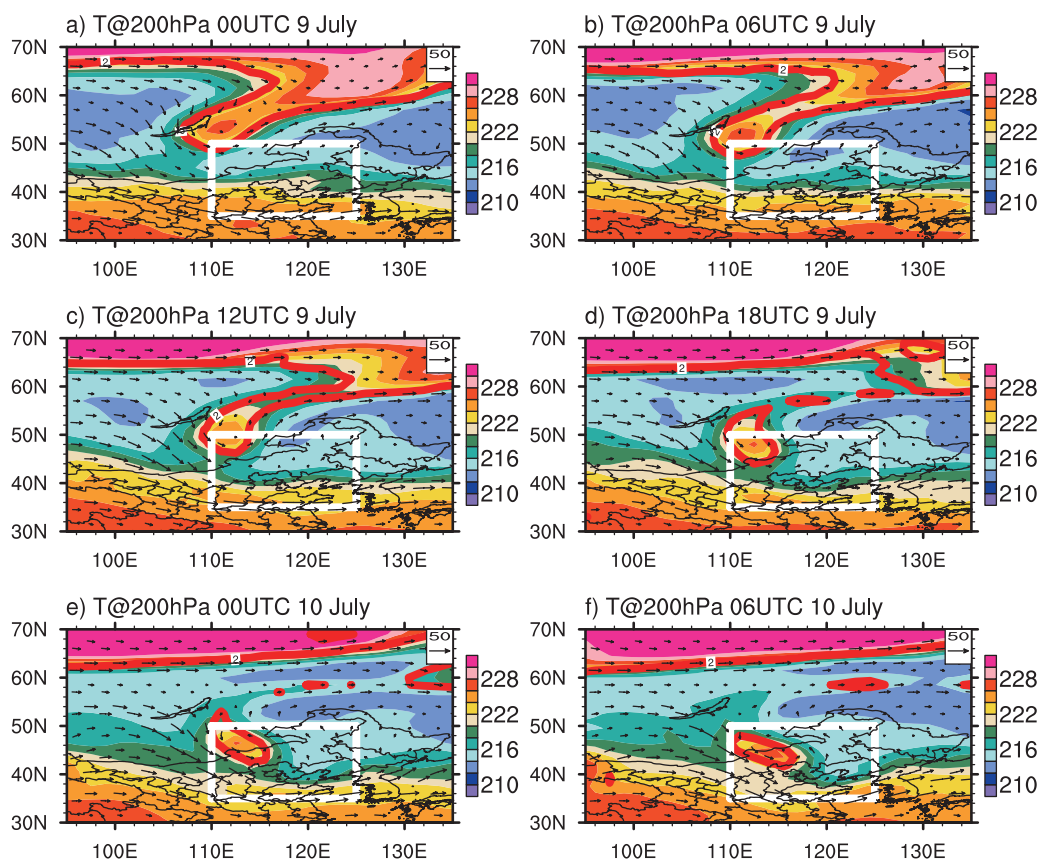
Fig. 4. The 6-h evolution of ERA-Interim temperature (shaded) and wind vectors at 200 hPa pressure surface and PV isoline (2 PVU) at 330 K isentropic surface: (a) 0000 UTC 9 July; (b) 0600 UTC 9 July; (c) 1200 UTC 9 July; (d) 1800 UTC 10 July; (e) 0000 UTC 10 July; (f) 0600 UTC 10 July 2007. Place of the COL occurrence is indicated by a white box.

growth of the upstream Siberian ridge, the isentropic PV trough extended southwestward and caused a pocket of warm air mass to be transported from the polar region to the Mongolian region (compare Figs. 4a–c and 2d). At 1800 UTC 9 July, the further development of the Siberian ridge cut the PV isoline from its polar origin (Fig. 4d), leading to an isolated warm-core cyclone moving slowly southward and hovering over northern China during the following 18 hs (Figs. 4d–f). The cutoff of polar stratospheric intrusion also caused the transport of warm polar stratospheric air into the mid-latitudes (see the remnant PV isolines near 60°N in Figs 4d–f).

4.2 *Impact of the Stratospheric Intrusion on the UTLS Ozone*

In this section, the impacts of stratospheric intrusion on ozone concentrations in the UTLS region and ozone STE are quantified using the retrieved profiles onboard several satellite instruments (MLS, HIRDLS, and OMI).

To illustrate the impact of stratospheric intrusion on UTLS ozone, Fig. 5 (upper four panels) facilitates a comparison of the along-track ozone concentration passing over the marked region in Figs. 1 and 2 before and during the event retrieved from MLS and HIRDLS observations (refer to Figs. 1a and f for the locations of each instrument's profiles). For example, on 5 July 2007, the westerly jet core was located near its summertime climatological latitudes (between 35°N and 40°N), with a maximum speed of >50 m s^{-1} (Figs. 5a and c). The tropopause break went through the jet core, descending from near 100 hPa southward of 35°N to ~200 hPa northward of 40°N. As a result, before the COL event, the ozone-rich air between 40°N and 50°N was generally confined above the 200 hPa pressure surface. On 10 July 2007, due to the southward excursion of polar stratospheric air during the development of the COL (Fig. 4), the westerly jet was greatly weakened and retreated southward to tropical latitudes (Figs. 5b and d). Due to the formation of the tropopause funnel (Fig. 3), dynamical tropopause
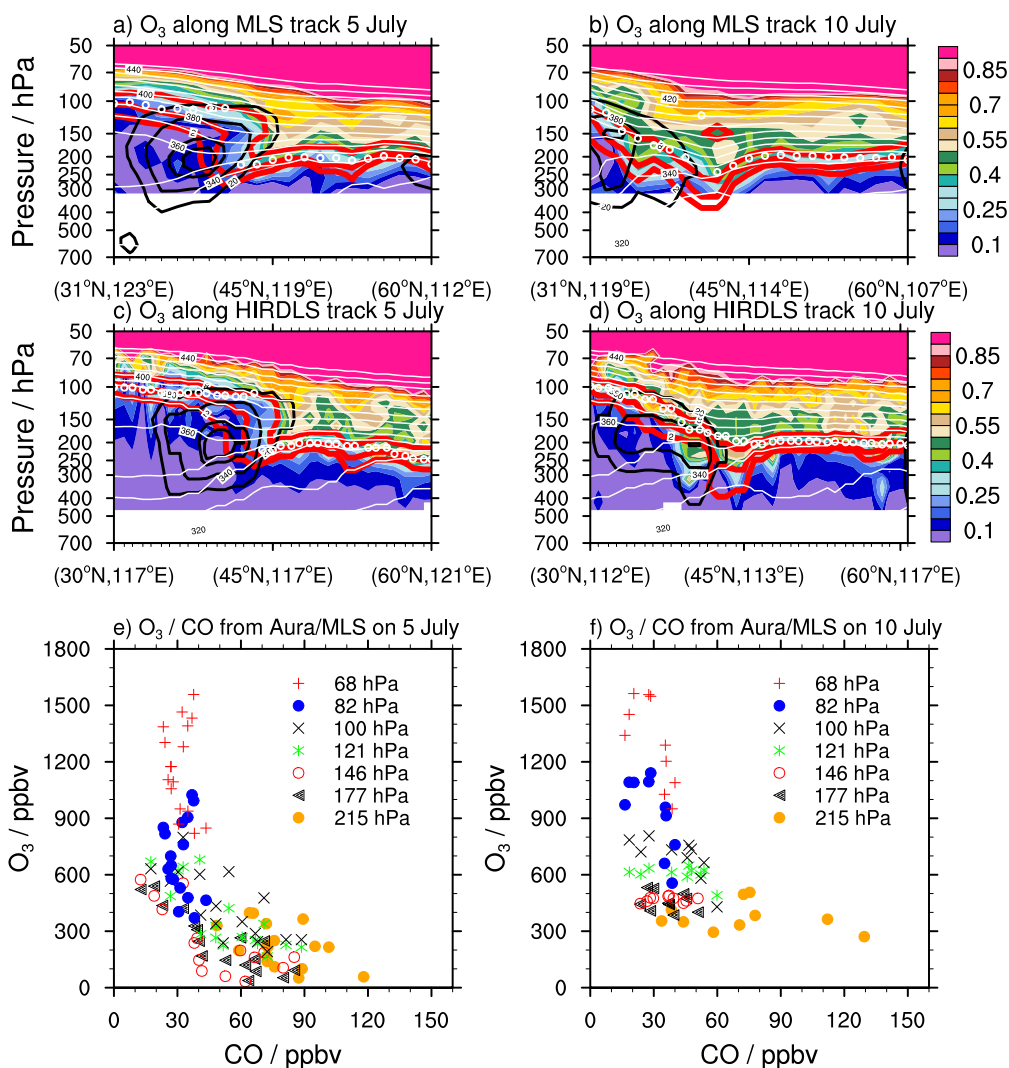
Fig. 5. (top) Observed ozone mixing ratio (Units: ppmv) and ERA-Interim potential temperature (white contours: K) near the tropopause before (on 5 July 2007) and after (on 10 July 2007) the COL occurrence along (a and b) MLS and (c and d) HIRDLS tracks passing over the marked region shown in Fig. 1. Same as Fig. 3, zonal wind speed (black solid contours), PV isolines (2, 4, and 8 PVU, red solid contours), and thermal tropopause (white circles) from ERA-Interim reanalysis are overlaid. (bottom) O_3–CO tracer-tracer correlation from MLS observations in the upper troposphere and lower stratosphere between 68 and 215 hPa (red plus: 68 hPa; blue dot: 82 hPa; black cross: 100 hPa; green asterisk: 121 hPa; red circle: 146 hPa; black triangle: 177 hPa; orange dot: 215 hPa) on (e) 5 July and (f) 10 July 2007 within the area of COL occurrence (marked by a white box).

(PV isolines) together with high ozone concentrations intruded to as low as 400 hPa (Fig. 5d). The tracer–tracer correlation, a common diagnostic tool to identify the mixing of air masses with different origins (e.g., Waugh et al., 1997; Pan et al., 2007), shows the impact of stratospheric intrusion on chemical trace gases (O_3 and CO) in the UTLS region (68–215 hPa) above the COL region (Figs. 5e and f). On 5 July 2007, the O_3 and CO concentrations in this region satisfied the compact correlation documented in previous literature (e.g., Fischer et al., 2000), indicating a robust distin-

guishability between troposphere and stratosphere before the COL occurrence (Fig. 5e). However, on 10 July 2007, the O_3–CO correlation loosened up, leading to the disappearance of high CO concentration and low O_3 concentrations in the lowermost five layers (i.e., 100, 121, 146, 177, and 215 hPa) (compare Figs. 5f with e). Although the vertical resolution of MLS measurements are relatively crude and the samplings are limited at these levels, the variation in the measured O_3–CO correlation is pronounced enough to qualitatively highlight the downward intrusion of
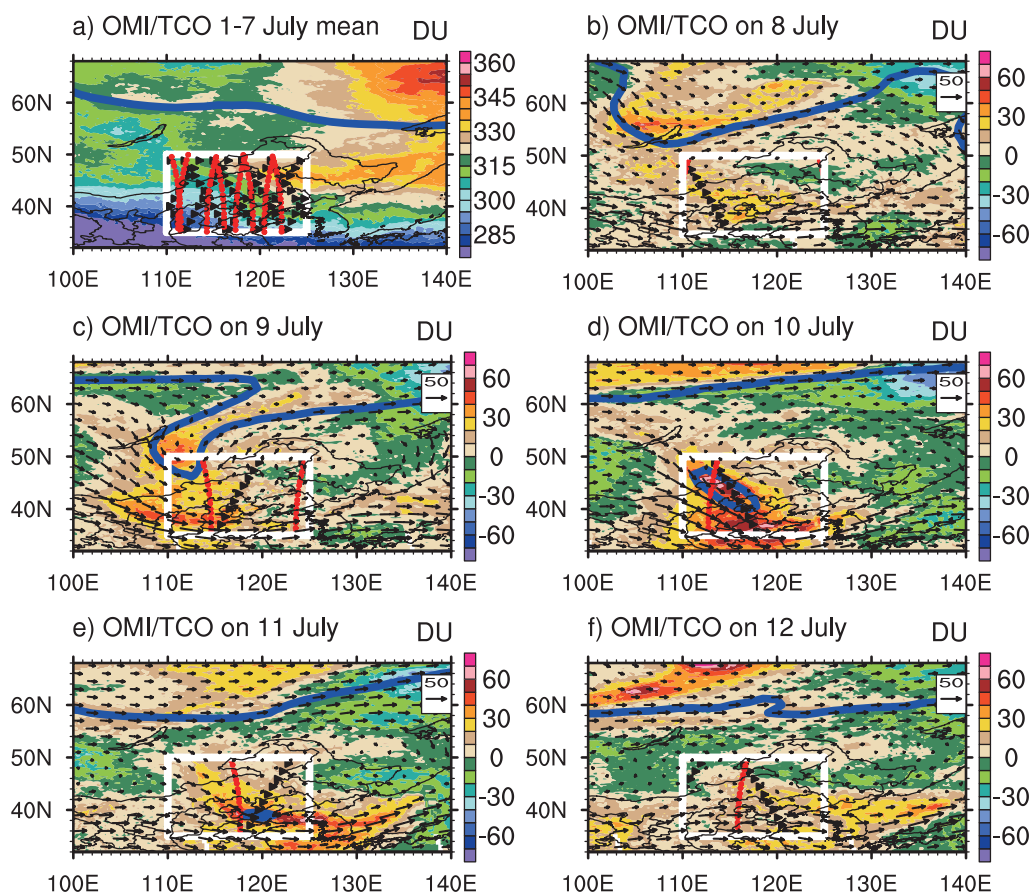
Fig. 6. Total column ozone (TCO) and its variation (Units: DU) observed by Ozone Monitoring Instrument over north China during the COL event: (a) 1–7 July 2007 mean; (b–f) daily variations from 8 to 12 July 2007 relative to the 1–7 July mean. Region of the COL occurrence is marked by a white box. Locations of MLS and HIRDLS profiles within the marked region are indicated by black triangles and red dots. Evolution of the 2-PVU PV isoline at 330 K and 200-hPa winds (Units: m s^{-1}) are overlaid with blue bold solid line and vectors.

stratospheric air from above the tropopause. Therefore, according to MLS measurements, the downward intrusion of stratospheric air can reach as deep as 215 hPa at least, which lies around the thermal tropopause (compared to thermal tropopause in Figs. 5a–d).

Figures 6b–f illustrate the daily variation of TCO (8–12 July 2007) relative to the 1–7 July average (Fig. 6a), together with the evolution of horizontal wind vectors at 200 hPa and the 2-PVU isentropic PV isoline at 330 K, which. As shown, there was a high correlation between the TCO increase and the PV isoline, which indicates an intrusion of stratospheric air. For example, on 8 July 2007, the 2-PVU isoline extended southward towards Baikal, leading to a pronounced increase (∼40 DU) in local TCO compared with the 1–7 July mean (Fig. 6b). With the equatorial excursion of the PV isoline, the area with TCO enhancement extended from Mongolia to northern China

(Figs. 6c and d). On 10 July 2007, as the COL reached its peak, the maximum TCO enhancement was up to 60–70 DU at the center of the stratospheric intrusion (Fig. 6d). When the COL began to decay, its impact on the local TCO weakened on 11 and 12 July (Figs. 6e and f).

Notably, there was an intensive TCO increase downstream the movement of the high-PV stratospheric air (e.g., Figs. 6c–f). Meanwhile, the distribution of these TCO increased areas agrees well with transport pattern of the 200-hPa horizontal winds. Based on OMI measurements, the decaying COL led to a broad area of TCO enhancement (20–40 DU) downstream of the stratospheric intrusion over northern China (Figs. 6e and f). This issue is further discussed in section 4.3.

To determine the impact of the COL event on the vertical distribution of ozone concentration, as in our
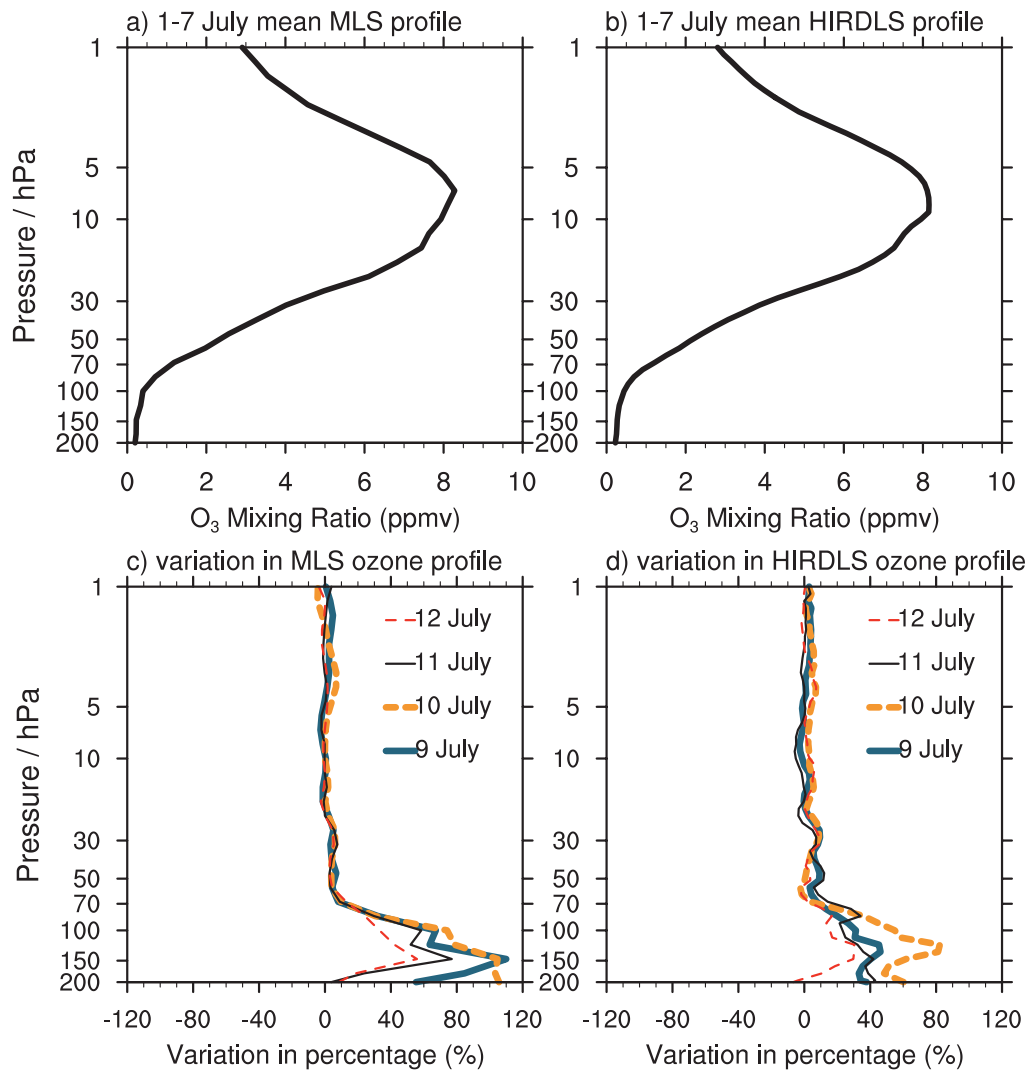
Fig. 7. (top) Reference ozone profile averaged in 1–7 July 2007 within the region of COL occurrence: results from (a) MLS observations; (b) HIRDLS observations. (bottom) percentage of daily variations in ozone profiles from 9 to 12 July 2007 relative to the reference ozone profile: results from (c) MLS observations; (d) HIRDLS observations.

previous studies (Liu et al., 2009, 2010), we averaged the daily ozone profiles from both MLS and HIRDLS measurements within the marked area (Fig. 6) to derive the daily variation in the ozone profile (Figs. 7c and d) relative to the reference profile (1–7 July average) (Figs. 7a and b). As shown in Figs. 7c and d, there was a pronounced ozone increase below 50 hPa throughout the COL event, with the maximum ozone increase (>80%) located near 150 hPa. In other words, the TCO enhancement on 9–12 July 2007 could be mostly attributed to the UTLS process related to the COL event, i.e., the formation of a "tropopause funnel" and associated STE. Figures 7c and d also indicate the temporal evolution of the dynamics contribut-

ing to ozone enhancement in the UTLS region. For example, as the stratospheric intrusion approached the marked region on 9 July (Fig. 6c), it led to a 40%–110% increase in the UTLS ozone concentration (Figs. 7c and d). When the intensity of the COL peaked on 10 July (Fig. 6d), the increase in UTLS ozone concentration between 100 and 150 hPa reached 80%–110% (Figs. 7c and d). In the COL's decaying phase, the ozone profile between 100 and 200 hPa recovered gradually on 11 and 12 July (Fig. 7d). The differences in the ozone variations between MLS and HIRDLS measurements could be generally related to their differences in sampling, vertical resolution, and precision in the UTLS region.
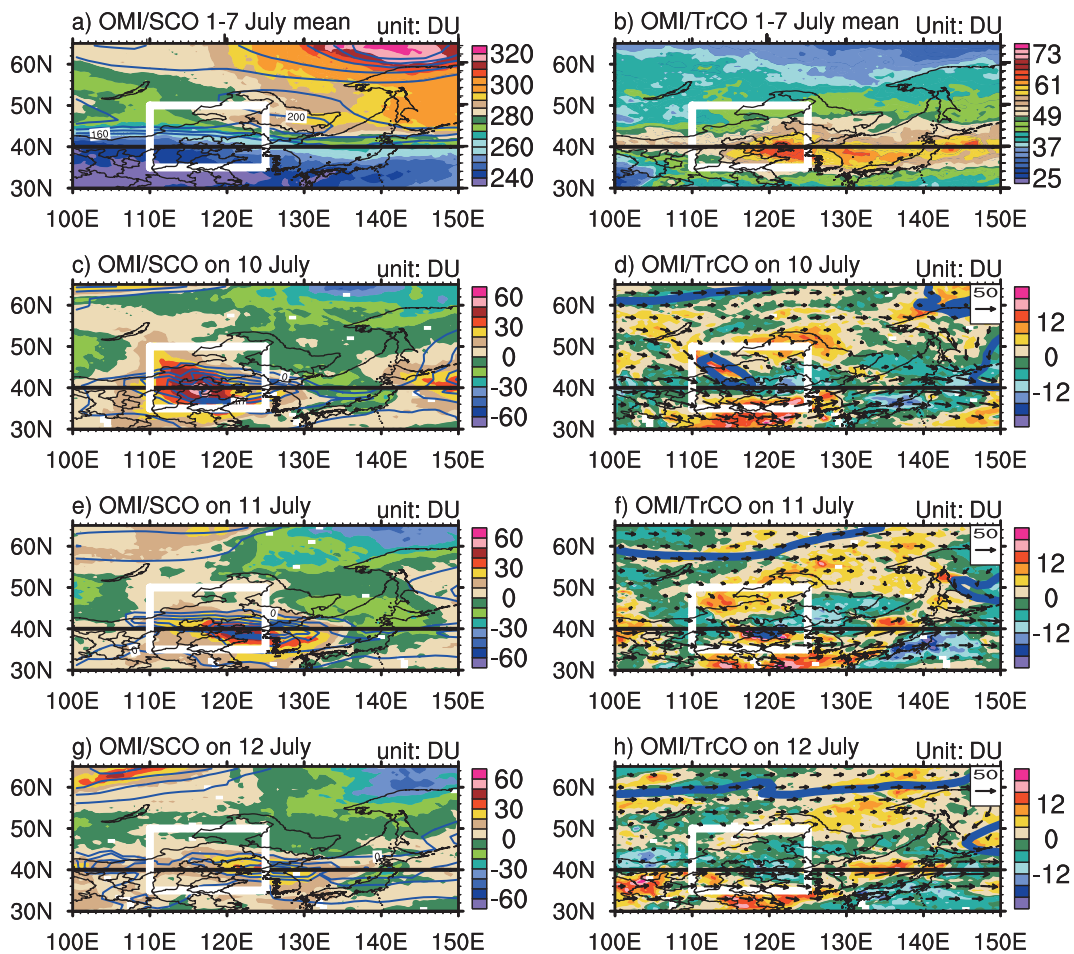
Fig. 8. (left panels) Stratospheric column ozone (SCO, Units: DU) from OMI retrievals and thermal tropopause pressure (Units: hPa) from ERA-Interim reanalysis. (right panels) Tropospheric column ozone (TrCO, Units: DU) from OMI retrievals and 200-hPa wind vectors from ERA-Interim (right panels): (a and b) 1–7 July mean; (c–h) daily variations from 10 to 12 July 2007 relative to the 1–7 July mean. Region of the COL occurrence is marked by a white box. Same as Fig. 6, the 2-PVU isentropic PV isoline is overlaid. Black solid line indicates the cross-section along 40°N to be shown in Fig. 9.

4.3   Characteristics of the irreversible ozone intrusion into the upper troposphere

Based on the OMI ozone profiles, we analyzed the characteristics of the irreversible ozone intrusion below the tropopause and quantify its contribution to the tropospheric column ozone (TrCO) throughout the COL event.

Figure 8 (left panels) shows the daily variations in OMI's SCO measurements and thermal tropopause pressure from ERA-Interim relative to the 1–7 July mean. There was a high correlation between the SCO increase and increase of the tropopause pressure (compare blue contours with shaded SCO contours in Figs. 8c, e, and g). These results suggest a dominant role of tropopause height decrease in controlling the SCO increase in this case. Figure 8 (right panels)

shows the daily variations of TrCO relative to the 1–7 July mean (Fig. 8b for the mean). The TrCO centers travelled along with the southward migration of the high-PV air mass (Figs. 8d and f) but lagged behind the motion of the SCO center (e.g., compare Figs. 8c with d). Meanwhile, it is noted that there is northward transport of high tropospheric ozone from south of 40°N, which contributes to the TrCO increase extending from East China towards the north Japan Sea on 11 and 12 July (Figs. 8d, f, and h). However, temporal evolution of the vertical velocity shows that the geographical pattern of the descent region agrees well the temporal evolution of the high TrCO during 8–10 July (not shown), which leads to the high TrCO to the south of 40°N on 10 July (Fig. 8d). Cross-sections of the vertical velocity further show the ex-

istence of the descents from 850 to 250 hPa during 8–10 July (not shown). Therefore, the high TrCO to the south is very likely produced by the persistently downward transport from lower stratosphere and subsequently southeastward advection at the rear of the cold tropospheric cyclone. During the following days (10–12 July), the high ozone concentrations are further transported northeastward ahead of the cyclone (Figs. 8f and h). However, quantitative ozone budget should be analyzed further using a detailed chemical transport model. The increase in TrCO (up to 12–16 DU) was only one third of the magnitude of the SCO increase (up to 40–50 DU; Figs. 8c and d). In other words, ∼75% of the local TCO increase might be attributable to the descent of the tropopause and downward transport of ozone into UTLS, whereas the other 25% of the TCO increase might have been contributed by the ozone STE below the bottom of the tropopause funnel. Meanwhile, there were still areas with pronounced TrCO enhancement to the south of the stratospheric intrusion associating with the high-PV air mass. And these ozone increases cannot be explained by the variation of tropopause height (compare each right panel with left one). Analysis of the 200-hPa horizontal winds shows that the distribution of TrCO enhancement agrees well with the pattern of upper tropospheric winds over East Asia. These results indicate a possibility that the stratospheric ozone intruded across the tropopause and was further transported downstream by the strong westerlies in upper troposphere. As a result, the area with TrCO enhancement extended from east China toward the north Japan Sea via South Korea on 11 and 12 July (Figs. 8f and h). This picture also agrees with previous studies (e.g., Gouget et al., 2000), which argues that the tropospheric ozone increase resulted from stratospheric ozone intrusion due to the erosion and mixing near the upper-level frontal structure.

Figure 9 shows the OMI ozone distribution along the 40°N cross-section, together with the ERA-Interim meteorology. As shown, due to the development of the tropopause funnel and high-level front, there was prominent ozone transport and mixing downward across the tropopause. For example, on 9 and 10 July 2007, the potential temperature contours between 100 and 300 hPa converged towards the thermal tropopause, indicating the development of the upper-level frontal structure (Figs. 9b and c). The vertical shift of lapse-rate tropopause can also be noted from the variation in the PV contours, which are conventionally regarded as the dynamic tropopause. Meanwhile, there were air masses with typical stratospheric ozone concentrations intruding across the thermal tropopause. With the approach of the COL system on 11 July 2007 (compare Figs. 9d with 8f), the tropopause funnel deepened, which led to ozone-rich air descending from above 100 hPa to the lowermost stratosphere at 200 hPa (Fig. 9d). During the following days, the tropopause funnel and frontal structure associated with the COL continued decaying (Figs. 9e and f), which led to pronounced ozone-rich air mixing downward below the tropopause. This situation is quite similar to the previous documentation of irreversible ozone STE in COL's decaying phases (e.g., Gouget et al., 2000). As a result, the high-rich air was diluted with the environment air mass and further transported downstream by the strong horizontal winds in upper troposphere (Figs. 9e and f), leading to TrCO enhancement to the east of 120°E, which is located downstream the decaying COL area (Figs. 8f and h).

5. Link between stratospheric intrusion and the intensifying of low-level cyclones

Previous theoretical studies (e.g., Hoskins et al., 1985) had shown that a positive PV anomaly in the upper troposphere can usually lead to prominent cyclogenesis well below. We investigated a possible link between the stratospheric intrusion of high PV and COL occurrence and evolution of the low-lying cyclone.

Figure 10 shows the development of geopotential height in the upper, middle, and lower troposphere and its relationship to stratospheric intrusion, which is denoted by the isentropic PV isoline. In the developing phase (0000 UTC 8 July), there was a relatively small and weak cyclone at 500 hPa and 700 hPa over northern China (Figs. 10d and g), but without any upper-level cyclone at 200 hPa (Fig. 10a). As shown in Figs. 1e and 2e, the rapid growth of an upstream Siberian ridge responsible for the pronounced stratospheric intrusion led to the emergence of a closed cyclone to the east of the Baikal region at 200 hPa, with a trough extending southward toward northern China at 500 hPa. Meanwhile, the cold-core cyclone at 700 hPa underwent pronounced growth, which can be regarded as a dynamical consequence of the upper-level PV intrusion, according to PV theory (Hoskins et al., 1985). At 1800 UTC 9 July, with the 200-hPa cyclone completely detached from its polar stratospheric origin, the newborn cyclone merged into the existing cyclone over northern China, leading to the former's rapid growth. Meanwhile, the 700-hPa cyclone showed further strengthening and enlargement.

6. Summary and discussion

In this study, the HIRDLS, MLS, and OMI measurements onboard the EOS-Aura satellite and the
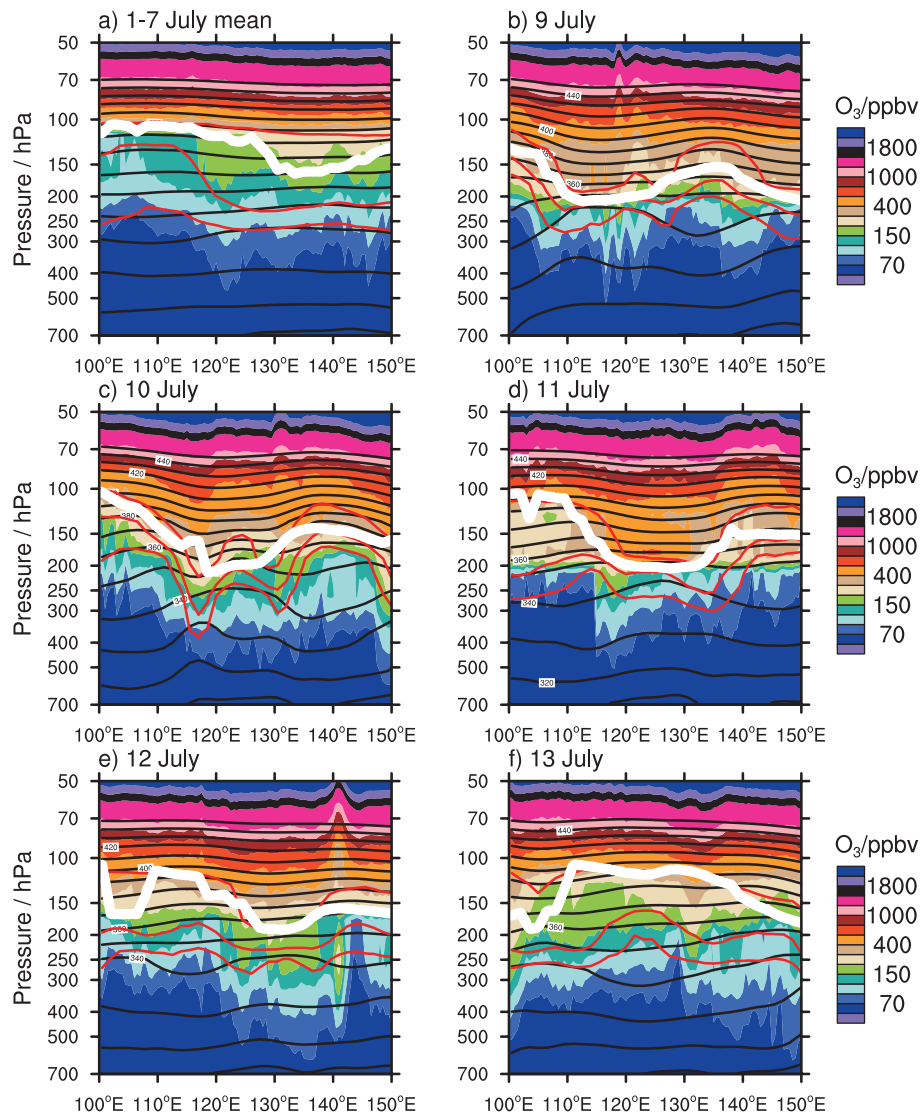
Fig. 9. Cross section of ozone concentration (units: ppbv) from OMI retrievals and ERA-Interim meteorology along 40°N cross-section indicated by solid line in Fig. 8: (a) 1–7 July mean; (b) 10 July; (c) 11 July; (d) 12 July 2007. ERA-Interim PV isolines (2, 4, and 6 PVU), potential temperature (interval: 10 K), and thermal tropopause (units: hPa) are overlaid with red, black, and white contours.

ERA-Interim meteorological analysis were used to analyze the characteristics of stratospheric intrusion during a COL event over northern China in early July 2007. The results showed that the COL system was characterized by a dipole structure extending from the lower troposphere to the lower stratosphere, with a deep cold cyclone in the middle and lower troposphere (below ∼300 hPa) and a shallow warm-core cyclone in the UTLS region (100–300 hPa). Meteorological analysis indicated a close connection between the warm-core structure in the UTLS region and the stratospheric intrusion from the warm polar stratosphere. As a result, there was a massive downward intrusion of ozone-rich stratospheric air below the funnel-shaped

tropopause (Figs. 5 and 9), leading to a maximum increase in the local TCO up to 40–70 DU when the COL peaked on 10 July. Ozone profiles from both HIRDLS and MLS measurements indicated that the TCO increase could be attributed to the ozone increase below 50 hPa (the lowermost stratosphere and troposphere). Ozone retrievals from OMI measurements indicated that variations in stratospheric and tropospheric ozone column contribute to ∼75% (up to 40–50 DU) and 25% (up to 12–16 DU) of the TCO increase, respectively. Further analysis showed that the SCO increase was highly related to the descent of the local tropopause throughout the lifetime of COL. However, the increase of TrCO was controlled by the
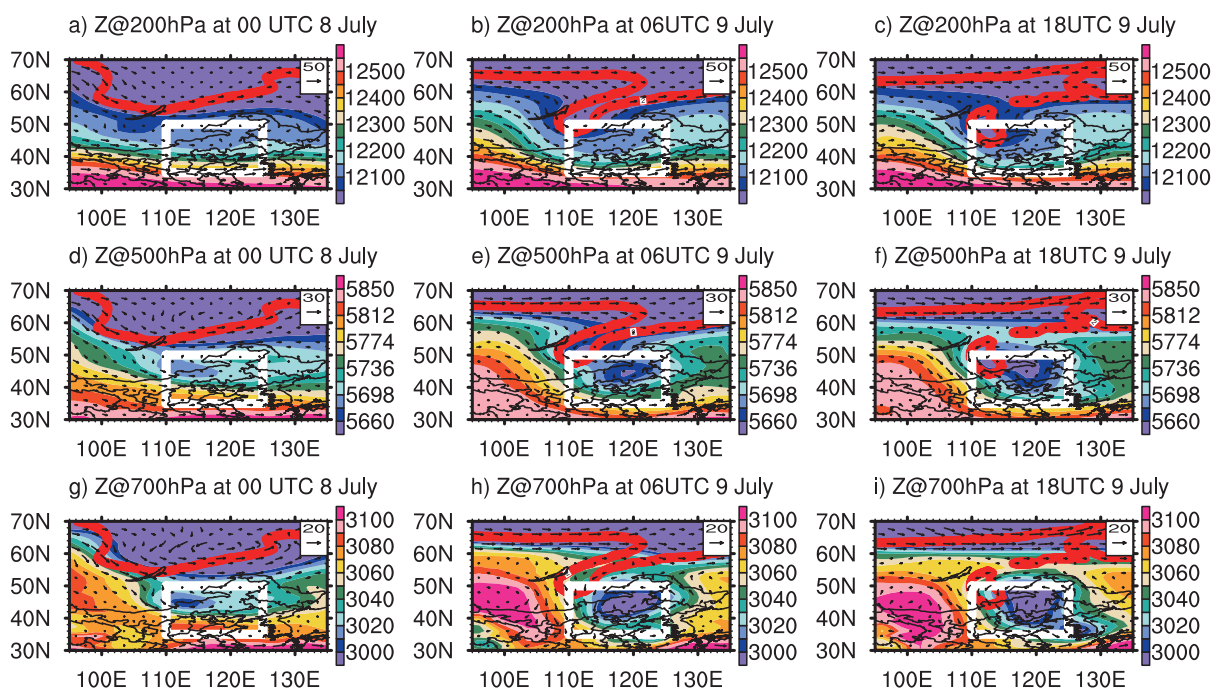
Fig. 10. ERA-Interim geopotential height (shaded: m) and wind vectors in (top) upper (200 hPa), (middle) middle (500 hPa), and (bottom) lower (700 hPa) troposphere at (a, d, and g) 0000 UTC 8 July, (b, e, and h) 0600 UTC 9 July, and (c, f, and i) 1800 UTC 9 July 2007. The red bold solid line indicates the 2-PVU isentropic PV isoline at 330 K. Location of the COL occurrence is indicated by a white box.

erosion of the tropopause funnel and mixing/transport near the upper-level front area ahead of the stratospheric intrusion. Therefore, there was another TrCO increase center ahead of the high-PV air mass (Figs. 8d and f). After the COL system began to decay on 11 July, the ozone-rich air was mixed with the environment and further transported downstream by the upper tropospheric winds, producing a large area with TrCO enhancement extending from east China toward the north Japan Sea via South Korea (Figs. 8f and h).

The picture in this case study agrees well with previous studies on ozone STE associated with COL system (e.g., Gouget et al., 2000). However, in such severe synoptic system as COL, the thermal tropopause might sometimes be incorrectly placed too high. Therefore, division of stratospheric and tropospheric ozone columns in this case study could be still far from perfect and the irreversible intrusion of stratospheric ozone into the upper troposphere might be, to some extent, overestimated. However, at the present time, there is rarely a better tropopause definition to replace the lapse-rate definition in our analysis. In addition, some recent studies (e.g., Kim and Lee, 2010) have argued that the springtime tropospheric ozone maximum over Northeast Asia was hardly associated with the contribution from stratospheric intru-

sion. But here we find that the stratospheric intrusion related to certain intense upper-level synoptic systems, such as the COL event, could be an important factor in the enhancement of tropospheric ozone abundance over Northeast Asia. However, more detailed modeling studies should be performed to quantify the irreversible transport and mixing of stratospheric ozone into the troposphere and their downstream impact on the tropospheric photochemistry (e.g., Tie and Hess, 1997; Lamarque et al., 1999). On the other hand, the different processes (e.g., tropopause descent, downward transport) leading to the increase of both SCO and TrCO (as shown in Fig. 8) should also be quantified using detailed transport model.

Analysis of the ERA-Interim meteorology showed dynamical linkage between the downward intrusion of high PV and the strengthening of the low-level cyclone. With the downward intrusion of stratospheric PV, a newborn cyclone merged with the existing cyclone over northern China, leading to rapid mid-tropospheric cyclone growth. As a result, the low-level cyclone at 700 hPa also underwent pronounced strengthening and enlargement. As described by PV theory (e.g., Hoskins et al., 1985), positive upper-level PV anomalies are supposed to cause rapid cyclogenesis at lower levels. Therefore, in the present study, the downward intru-

sion of stratospheric PV related to the COL event could be one of the major factors leading to the rapid development of low-level cyclones. However, more mechanisms need to be investigated to explain the dynamical development of low-level cyclones and their relationship to neighboring synoptic systems.

REFERENCES

Ancellet, G., M. Beekmann, and A. Papayannis, 1994: Impact of a cutoff low development on downward transport of ozone in the troposphere. *J. Geophys. Res.*, **99**, 3451–3468, doi: 10.1029/93JD02551.

Bell, G. D., and L. F. Bosart, 1989: A 15-year climatology of Northern Hemisphere 500 mb closed cyclone and anticyclone centers. *Mon. Wea. Rev.*, **117**, 2142–2163.

Fischer, H., and Coauthors, 2000: Tracer correlations in the northern high latitude lowermost stratosphere: Influence of cross-tropopause mass exchange. *Geophys. Res. Lett.*, **27**, 97–100.

Gille, J. C., J. J. Barnett, J. C. Whitney, M. A. Dials, D. M. Woodard, W. Rudolf, A. Lambert, and W. Mankin, 2003: The High Resolution Dynamics Limb Sounder (HIRDLS) experiment on Aura. Proc. *SPIE Int. Soc. Opt. Eng.*, **5152**, 162–171, doi: 10.1117/12.507657.

Gille, J., and Coauthors, 2008: High resolution dynamics limb sounder: Experiment overview, recovery, and validation of initial temperature data. *J. Geophys. Res.*, **113**, D16S43, doi: 10.1029/2007JD008824.

Gimeno, L., R. M. Trigo, P. Ribera, and J. A. Garcia, 2007: Editorial: Special issue on cutoff low system (COL). *Meteor. Atmos. Phys.*, **96**, 1–2.

Gouget, H., G. Vaughan, A. Marenco, and H. G. J. Smit, 2000: Decay of a cutoff low and contribution to stratosphere-troposphere exchange. *Quart. J. Roy. Meteor. Soc.*, **126**, 1117–1141.

HIRDLS Team, cited 2010: High Resolution Dynamics Limb Sounder (HIRDLS) Earth Observing System (EOS) Data description and quality version 5 (V5). [Available online at http:/disc.sci.gsfc.nasa.gov/ Aura/data-holdings/HIRDLS/documents/HIRDLS-V5-DQD.pdf]

Holton, J. R., P. H. Haynes, M. E. McIntyre, A. R. Douglass, R. B. Rood, and L. Pfister, 1995: Stratosphere-troposphere exchange. *Rev. Geophys.*, **33**, 403–439.

Hoskins, B. J., M. E. McIntyre, and A. W. Robertson, 1985: On the use and significance of isentropic potential vorticity maps. *Quart. J. Roy. Meteor. Soc.*, **111**, 877–946.

Hsieh, Y. P., 1949: An investigation of a selected cold vortex over North America. *J. Meteor.*, **6**, 401–410.

Hu, K., R. Lu, and D. Wang, 2010: Seasonal climatology of cutoff lows and associated precipitation patterns over Northeast China. *Meteor. Atmos. Phys.*, **106**, 37–48.

Kentarchos, A. S., and T. D. Davies, 1998: A climatology of cutoff lows at 200 hPa in the Northern Hemisphere, 1990–1994. *Int. J. Climatol.*, **18**, 379–390.

Kentarchos, A. S., G. J. Roelofs, J. Lelieveld, and E. Cuevas, 2000: On the origin of elevated surface ozone concentrations at Izana Observatory, Tenerife during late March 1996. *Geophys. Res. Lett.*, **27**, 3699–3702, doi: 10.1029/2000GL011518.

Kim, J. H., and H. Lee, 2010: What causes the springtime tropospheric ozone maximum of Northeast Asia? *Adv. Atmos. Sci.*, **27**, 543–551, doi: 10.1007/s00376-009-9098-z.

Lamarque, J.-F., P. G. Hess, and X. X. Tie, 1999: Three-dimensional model study of the influence of stratosphere-troposphere exchange and its distribution on tropospheric chemistry. *J. Geophys. Res.*, **104**, 26363–26372, doi: 10.1029/1999JD900762.

Levelt, P. F., and Coauthors, 2006: Science objectives of the ozone monitoring instrument. *IEEE Trans. Geosci. Remote Sens.*, **44**, 1199–1208.

Livesey, N. J., and Coauthors, 2007: Earth Observing System (EOS) Aura Microwave Limb Sounder (MLS) Version 2.2 Level 2 data quality and description document, Tech. Rep. D-33509, Jet Propul. Lab., Pasadena, California, 109pp

Livesey, N. J., and Coauthors, 2008: Validation of Aura Microwave Limb Sounder O_3 and CO observations in the upper troposphere and lower stratosphere. *J. Geophys. Res.*, **113**, D15S02, doi: 10.1029/2007JD008805.

Livesey, N. J., and Coauthors, 2011: Earth Observing System (EOS) Aura Microwave Limb Sounder (MLS) Version 3.3 Level 2 data quality and description document, Tech. Rep. D-33509, Jet Propul. Lab., Pasadena, California.

Liu, C., Y. Liu, Z. Cai, S. Gao, D. Lü, and E. Kyrölä, 2009: A Madden-Julian Oscillation-triggered record ozone minimum over the Tibetan Plateau in December 2003 and its association with stratospheric "low-ozone pockets". *Geophys. Res. Lett.*, **36**, L15830, doi: 10.1029/2009GL039025.

Liu, C., Y. Liu, Z. Cai, S. Gao, J. Bian, X. Liu, and K. Chance, 2010: Dynamic formation of extreme ozone minimum events over the Tibetan Plateau during northern winters 1987–2001. *J. Geophys. Res.*, **115**, D18311, doi: 10.1029/2009JD013130.

Liu, X., P. K. Bhartia, K. Chance, R. J. D. Spurr, and T. P. Kurosu, 2010a: Ozone profile retrievals from the Ozone Monitoring Instrument. *Atmos. Chem. Phys.*, **10**, 2521–2537.

Liu, X., P. K. Bhartia, K. Chance, L. Froidevaux, R. J. D. Spurr, and T. P. Kurosu, 2010b: Validation of Ozone Monitoring Instrument (OMI) ozone profiles and stratospheric ozone columns with Microwave Limb Sounder (MLS) measurements. *Atmos. Chem. Phys.*, **10**, 2539–2549.

Nardi, B., and Coauthors, 2008: Initial validation of ozone measurements from the High Resolution Dynamics Limb Sounder. *J. Geophys. Res.*, **113**, D16S36, doi: 10.1029/2007JD008837.

Nieto, R., and Coauthors, 2005: Climatological features of cutoff low systems in the Northern Hemisphere. *J. Climate*, **18**, 3085–3103.

Nieto, R., M. Sprenger, H. Wernli, R. M. Trigo, and L. Gimeno, 2008: Identification and climatology of cutoff lows near the tropopause. *Annals of the New York Academy of Sciences*, **1146**, 256–290.

Palmén, E., 1949: Origin and structure of high-level cyclones south of the maximum westerlies. *Tellus*, **1**, 22–31.

Palmén, E., and C. W. Newton, 1969: *Atmospheric Circulation System: Their Structure and Physical Interpretation.* Academic Press, New York, 603pp.

Pan, L. L., J. C. Wei, D. E. Kinnison, R. R. Garcia, D. J. Wuebbles, and G. P. Brasseur, 2007: A set of diagnostics for evaluating chemistry-climate models in the extratropical tropopause region. *J. Geophys. Res.*, **112**, D09316, doi: 10.1029/2006JD007792.

Parker, S. S., J. T. Hawes, S. J. Colucci, and B. P. Hayden, 1989: Climatology of 500 mb cyclones and anticyclones, 1950–85. *Mon. Wea. Rev.*, **117**, 558–571.

Peltonen, T., 1963: A case study of an intense upper cyclone over eastern and northern Europe in November 1959. *Geophysica*, **8**, 225–251.

Pittman, J. V., and Coauthors, 2009: Evaluation of AIRS, IASI, and OMI ozone profile retrievals in the extratropical tropopause region using in situ aircraft measurements. *J. Geophys. Res.*, **114**, D24109, doi: 10.1029/2009JD012493.

Price, J. D., and G. Vaughan, 1992: Statistical studies of cutoff low systems. *Ann. Geophys.*, **10**, 96–102.

Price, J. D., and G. Vaughan, 1993: On the potential for stratosphere-troposphere exchange in cutoff-low systems. *Quart. J. Roy. Meteor. Soc.*, **119**, 343–365.

Sato, T., 1951: On the structure of cold vortex. *Pap. Meteor. Geophys.*, **3**, 157–171.

Simmons, A., S. Uppala, D. Dee, and S. Kobayashi, 2007a: ERA-Interim: New ECMWF reanalysis products from 1989 onwards. *ECMWF Newsletter*, **110**, 25–35.

Simmons, A., S. Uppala., and D. Dee, 2007b: Update on ERA-Interim. *ECMWF Newsletter*, **111**, 5–5.

Sprenger, M., H. Wernli, and M. Bourqui, 2007: Stratosphere-troposphere exchange and its relation to potential vorticity streamers and cutoffs near the extratropical tropopause. *J. Atmos. Sci.*, **64**, 1587–1602.

Stohl, A., and Coauthors, 2003: Stratosphere-troposphere exchange: A review, and what we have learned from STACCATO. *J. Geophys. Res.*, **108**, 8516, doi: 10.1029/2002 JD002490.

Tao, S. Y., 1980: *The Heavy Rain in China.* Chinese Science Press, Beijing, 255pp. (in Chinese)

Tie, X., and P. Hess, 1997: Ozone mass exchange between the stratosphere and troposphere for background and volcanic sulfate aerosol conditions. *J. Geophys. Res.*, **102**, 25487–25500, doi: 10.1029/97JD01842.

Waugh, D. W., and Coauthors, 1997: Mixing of polar vortex air into middle latitudes as revealed by tracer-tracer scatterplots. *J. Geophys. Res.*, **102**, 13119–13134.

Waters, J. W., and Coauthors, 2006: The Earth Observing System Microwave Limb Sounder (EOS MLS) on the Aura satellite. *IEEE Trans. Geophys. Remote Sens.*, **44**, 1075–1092.

Wirth, V., 1995: Diabatic heating in an axisymmetrical cutoff cyclone and related stratosphere troposphere exchange. *Quart. J. Roy. Meteor. Soc.*, **121**, 127–147.

World Meteorological Organization, 1957: Meteorology–a three-dimensional science: Second session of the Commission for Aerology. *WMO Bulletin*, **4**(4), 134–138.

Yang, J., and D. Lü, 2003: A simulation study of stratosphere-troposphere exchange due to cutoff-low over Eastern Asia. *Chinese J. Atmos. Sci.*, **27**, 1031–1044. (in Chinese)

Zhang, C., Q. Zhang, Y. Wang, and X. Liang, 2008: Climatology of warm season cold vortices in East Asia: 1979–2005. *Meteor. Atmos. Phys.*, **100**, 291–301.

Zhao, S. X., and J. H. Sun, 2007: Study on cutoff low-pressure systems with floods over Northeast Asia. *Meteor. Atmos. Phys.*, **96**, 159–180.